Optical Nonlinearities and Molecular Kinetics of Hypocrellin A

Xiaoming Shang,* Guilan Zhang, Yunqi Liu, Guoqing Tang, and Wenju Chen

Institute of Modern Optics, Nankai University, Tianjin 300071, China

Received: January 27, 1998; In Final Form: June 8, 1998

Optical nonlinearities (including nonlinear absorption and nonlinear refraction) and the temporal properties of the nonlinear refraction of hypocrellin A (HA) in its resonant region have been investigated by using single-beam *Z*-scan and time-resolved two-color *Z*-scan techniques with picosecond pulses. The reverse saturable absorption effect can be attributed to the efficient absorption of excited states of both the normal and tautomeric forms, S_1 and S_1', with the contribution of S_1 as the dominant mechanism. The change of the refractive index of HA increases with increasing irradiance I_0 at low irradiances (<5 GW/cm^2), while it hardly changes with I_0 at high irradiances. The explanation for such an experimental phenomenon is that the averaged population densities of both S_1 and S_1' increase with I_0 at low irradiance, while those of these two states become saturated at high irradiance. The refractive nonlinearities exhibit a very slowly decaying tail, which is attributed to the contributions of S_1, S_1', and the triplet state of the normal form, T_1, and is dependent on the rise times and lifetimes of these intermediate states. The kinetic model for HA allows for the determination of the absorption cross sections of the ground state of the normal form of HA S_0, the ground state of its tautomer S_0', the excited state of its tautomer S_1', and the refractive nonlinearities of S_1, S_1', and T_1. The close match between the theory and experiment not only shows the completeness of the five-level kinetic model but also demonstrates the close relationship between the optical nonlinearities of HA and the dynamics involved in excited-state intramolecular proton transfer.

1. Introduction

Hypocrellin A (HA, Figure 1) is a natural perylene quinonoid pigment that has been used for centuries as folk medicine to cure various skin diseases and tumors in China.[1] Recently, it has also been shown that HA possesses extremely high toxicity toward enveloped lentiviruses. An example of this insidious type of virus is the human immunodeficiency virus.[2] Therefore, much attention has been directed toward the investigation of the photophysics and photochemistry of HA for the purpose of developing a scientific basis for ultimate understanding of antivirus principles.[1−7]

Although several studies have been done on HA, it should be noted that most of them only focused on its chemical properties as a singlet oxygen sensitizer and its photophysical properties as a light-induced antiviral agent. These studies used steady-state and transient spectroscopic techniques.[1−8] However, few of them focused on the studies of the nonlinear optical properties of HA.

Furthermore, our previous results showed that HA is a promising nonlinear optical material.[9] Therefore, from this point of view, the intensive study of its nonlinear optical properties is significant. On the other hand, it has been demonstrated that HA will undergo an intramolecular proton transfer in the excited state of its tautomer to produce the excited state of the normal form. Such a process will result in the population and relaxation of several electronic states, which cause the change in the third-order susceptibility of the molecule. Therefore, it is an effective way to investigate the dynamic processes of the molecule by studying its optical nonlinearities and their temporal properties.[10−12] Although we have recently reported the studies of optical nonlinearities of HA with the excitation of nanosecond pulses by a single-beam *Z*-scan technique,[9] its dynamics and optical nonlinearities with the excitation of picosecond pulses still require investigation for the following reasons. First, it has been shown that the time constant of excited-state intramolecular proton transfer (ESIPT) of HA is on the time scale of tens to hundreds of picoseconds and is dependent on the viscosity of solvent.[5,6] With longer, nanosecond pulses, the ESIPT process can be neglected because its rate is very fast relative to the duration of the excitation pulse. Therefore, a three-level model is a perfect approximation to its photophysical processes.[9] On the contrary, with the shorter, picosecond pulses and a solvent of low viscosity (e.g., ethanol), the ESIPT is important because its rate is comparable to the duration of the excitation pulse. As a result, a more complicated, five-level kinetic model is appropriate. This model allows for the determination of the linear and nonlinear optical parameters of

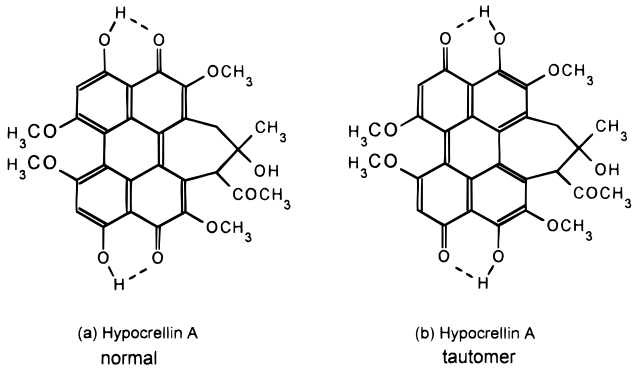

Figure 1. Two-dimensional structures of the normal form (a) and the tautomer form (b) of HA.

* To whom correspondence should be addressed. Present address: The University of Chicago, Department of Chemistry, 5735 S. Ellis Avenue, Chicago, IL 60637. E-mail: xshang@rainbow.uchicago.edu.

S1089-5639(98)00902-5 CCC: $15.00
Published on Web 08/28/1998

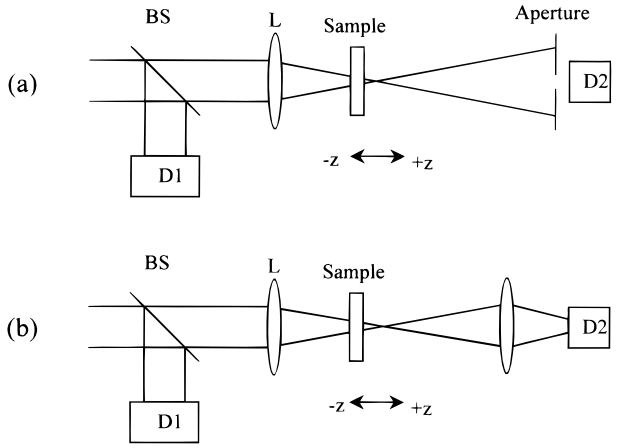

Figure 2. Schematic diagram for *Z*-scan setup showing both the closed aperture (a) and open aperture (b) configurations.

the tautomer and the attainment of useful information about the transient properties of the electronic states of the tautomer. This knowledge cannot be extended by use of the three-level model. Further, in our previous work, we did not give the time response of optical nonlinearities because only a single-beam *Z*-scan technique was involved in and the nanosecond pulse width was much larger than the time constants of some relaxation processes of HA. With picosecond pulse excitation, this kind of important information can be obtained by using a recently developed technique, time-resolved *Z*-scan.[12−15] Consequently, it is necessary to study the optical nonlinearities of HA with the excitation of picosecond pulses.

Also worthy of a special mention is that the quantitative study of the photophysics of HA is in progress,[5−8] and further work is still needed. As a matter of fact, one of the main goals of this paper is to deal with this issue. That is, with the numerical simulation of the kinetics of HA based on an appropriate model in order that the further understanding of its photophysical processes can be achieved.

In this paper, for the first time to our knowledge, the experimental and theoretical studies of the optical nonlinearities of HA obtained through excitation by picosecond pulses in its resonant region are reported. Both the nonlinear absorption and nonlinear refraction of HA were conveniently investigated by the single-beam *Z*-scan technique. Then, the temporal properties of nonlinear refraction of HA were also obtained by time-resolved two-color *Z*-scan measurements. In addition, based on a five-level kinetic model, we determined the nonlinear optical parameters of several states. Furthermore, the relationship between the optical nonlinearities of HA and its dynamics was also discussed.

***Z*-Scan Technique.** The *Z*-scan technique is a simple and sensitive method based on the principle of spatial beam distortion. It has been used to measure the sign and the magnitude of nonlinear refraction and nonlinear absorption of variety of materials.[16−21]

The schematic diagram for *Z*-scan measurement is shown in Figure 2. The transmittance of a tightly focused Gaussian beam through a finite aperture in the far field is measured as a function of the sample position *Z* with respect to the focal plane—hence the name closed aperture *Z*-scan (see Figure 2a). With the absence of nonlinear absorption, the closed aperture transmittance depends on the sign and the magnitude of refractive nonlinearity, represented by the change of the refractive index, Δn. For an optically thin sample[16] (thickness smaller than the diffraction length of the focused beam) with $\Delta n < 0$, the *Z*-scan curve, the sample transmittance versus sample position, exhibits a dispersion-like configuration with a peak followed by a valley. This can be explained by a simple physical model—optically induced lensing effect. When the sample is far from the focus and closer to the lens ($Z < 0$), the irradiance is low; no nonlinear process occurs. Therefore, the transmittance through the aperture is fairly constant with *Z* in this regime. As the sample is moved closer and closer to the focus, the irradiance increases, inducing a negative lensing effect with a varying focal length. This induced negative lens tends to collimate the laser beam and results in an increase in the aperture transmittance. At the focal position ($Z = 0$), the sample can be seen as equivalent to a thin lens positioned at the focus, which does not change the beam feature. Therefore, the sample transmittance at this position is similar to that far from the focus. Immediately after the focus ($Z > 0$), the defocusing due to the negative lensing effect causes a beam divergence, leading to decreased transmittance through the aperture. As the sample is moved far from the focus (large positive *Z*), the nonlinear refraction become negligible because of the low irradiance and the sample transmittance returns to its linear value, which is independent of *Z*. Therefore, the *Z*-scan curve shows a peak−valley configuration with $\Delta n < 0$. For a sample with a positive refractive nonlinearity, a positive lensing effect will be induced when the sample is closer to the focus. A similar analysis shows that the *Z*-scan curve is characterized by a prefocal minimum transmittance followed by a postfocal maximum. It should be noted that the sign of refractive nonlinearity can be determined simply by examining the configuration of a *Z*-scan curve.

Besides closed aperture *Z*-scan, there is another kind of *Z*-scan measurement called open aperture *Z*-scan. In this case, by removing the aperture and collecting all the transmitted light on detector D2, one can measure sample transmittance as a function of *Z* (see Figure 2b). Such a measurement can provide useful information about nonlinear absorption of material. If a sample exhibits purely refractive nonlinearity, the open aperture *Z*-scan curve shows a flat response. However, if nonlinear absorption is present, the *Z*-scan curve is quite different. The presence of saturation absorption will result in a symmetric peak configuration with respect to the focal position, whereas the presence of multiphoton absorption or reverse saturation absorption will give rise to a symmetric valley configuration, which has a minimum at $Z = 0$. It is worth noting that nonlinear absorption has some effect on the closed aperture *Z*-scan curves. For example, saturation absorption enhances the peak and suppresses the valley of a closed aperture *Z*-scan curve, whereas multiphoton absorption or reverse saturation absorption results in the opposite trend; i.e., it suppresses the peak and enhances the valley. There is a simple way to separate the contribution of nonlinear absorption to closed aperture *Z*-scan measurements under the certain conditions.[16] That is, the closed aperture *Z*-scan data are divided by the open aperture *Z*-scan data point by point. The newly obtained curve depends only on purely nonlinear refraction. The analysis methods of *Z*-scan data have been given in detail in several literature sources.[16,17]

In this work, we also employed a new technique, time-resolved two-color *Z*-scan, which was developed on the basis of single-beam *Z*-scan. It can not only measure nondegenerate nonlinear refraction and nonlinear absorption simultaneously but also provide temporal information about the optical nonlineairies of material. The unique advantage of this technique is that it allows us to distinguish mechanisms with different time responses and to study them separately.[13] Experimentally, this technique involves two laser beams with a variable time delay

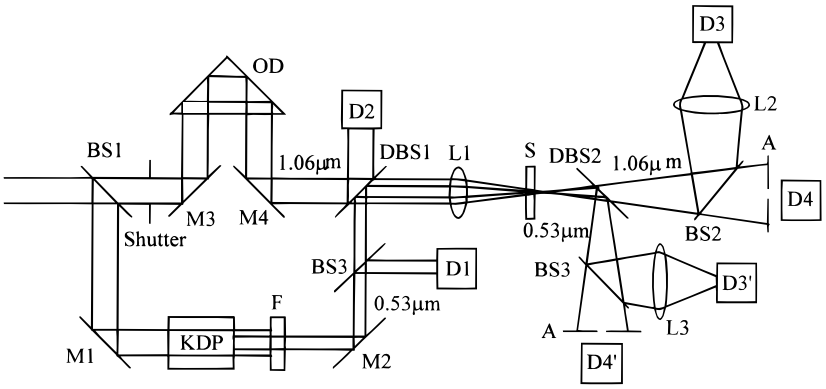

Figure 3. Experimental scheme for the single-beam and time-resolved two-color *Z*-scan techniques. BS1, BS2, BS3, and BS4 are beam splitters; M1, M2, M3, and M4 are mirrors; L1, L2, and L3 are lenses; DBS1 and DBS2 are dichroic beam splitters; OD is an optical-delay stage; KDP is the second-harmonic generator; D1, D2, D3, D4, D3′, and D4′ are detectors; F is the filter that transmits only 0.53 μm light.

between them. The stronger one, called the excitation beam, is used to generate the nonlinear effect, while the other weaker beam, referred to as the probe beam, is used to "read out" such a nonlinear effect. The actual experimental arrangement is shown in Figure 3. The detailed theoretical description for this technique will be provided in discussion section.

2. Experiment

2.1. Sample Preparation. HA was isolated from the fungus sacs of *Hypocrella bambusae* and recrystallized twice from benzene−petroleum ether before use. Greater than 98% purity (determined by TLC and NMR) of the HA sample was obtained. Spectrograde ethanol (Aldrich) was used as the solvent without further purification. The concentration of HA in ethanol used in this study was 2.5×10^{-4} M.

2.2. Experimental Arrangement. The experimental apparatus, shown in Figure 3, can perform both the single-beam and time-resolved two-color *Z*-scan measurements. The excitation light source was a home-built mode-locked Nd:YAG laser operating in TEM_{00} mode and producing pulses of 40 ps (fwhm) with a repetition rate of 1 Hz. The 1.06 μm single pulse from the laser is separated into two beams by a beam splitter BS1. The weaker probe beam passes through a variable optical delay line OD, while the other stronger beam goes through a KDP crystal to produce the second harmonic pulse (0.53 μm). This 0.53 μm output is used as the excitation light. These two beams are recombined by a dichroic beam splitter, DBS1, and then focused with a nearly achromatic lens of focal length $f = 212.3$ mm into the sample. These transmitted beams are separated by another dichroic beam splitter DBS2, causing the 0.53 μm light to be entirely reflected and the 1.06 μm light to be transmitted. This transmitted 1.06 μm light is then split by a beam splitter BS2, allowing for the measurement of the two-color closed and open aperture *Z*-scan signals simultaneously. Moreover, we can conveniently use the 0.53 μm beam reflected by DBS 2 to perform the closed and open aperture single-beam *Z*-scans. D1, D2, D3, D4, D3′, and D4′ are the probes of the laser energy meter (Laser Precision, Rj 7200). D1 and D2 are used to monitor the pulse energies of the excitation light and the probe light, respectively. D3 and D4 are used to detect the two-color *Z*-scan signals of open and closed aperture measurements, respectively. D3′ and D4′ are used to measure the single-beam *Z*-scan signals of open and closed aperture, respectively. The length of the sample is 400 μm. We used an aperture with a linear transmittance of $s = 0.1$, defined as the ratio of the pulse energy passing through the aperture to the total pulse energy, for all the closed aperture measurements given in this paper. Each of the experimental data points was obtained by averaging at least 10 shots. All the measurements were performed at room temperature.

By performing single-beam *Z*-scans at 0.53 and 1.06 μm on a standard sample, CS_2, we found a distance of 1.7 mm between the focal plane of the two beams because of chromatic aberration of lens L1. In addition, the waist radiuses were determined to be 24 and 30 μm for the 0.53 and 1.06 μm beams, respectively.

Before performing the two-color *Z*-scan experiment, several careful calibrations are required. First, adjustment of the incident pulse energy is necessary in order to ensure that the individual incidental probe light does not produce any nonlinear effect in the sample. The single-beam *Z*-scan method is used for this measurement. Second, the accurate spatial overlap between the excitation and probe beams at the focal positions must be achieved, and the precise position of the zero time delay between the two beams must also be located.[12,13]

3. Results

3.1. Single-Beam *Z*-Scan. With the excitation at 0.53 μm, we recorded nine series of *Z*-scan curves at nine different peak-on-axis irradiances at focuses, I_0. One of them for the case of $I_0 = 25$ GW/cm^2 is shown in Figure 4.

As is shown in Figure 4a, the normalized transmittance curve of an open aperture *Z*-scan exhibits a symmetrical valley with respect to $Z = 0$, which implies the presence of nonlinear absorption in HA solution at 0.53 μm. After confirming that the solvent, ethanol, does not exhibit nonlinear absorption under the same experimental conditions, we conclude that the observed nonlinear absorption should originate from HA. Furthermore, because the wavelength of excitation light (0.53 μm) is located on the red side of the resonant absorption peak of HA (see Figure 5), this observed nonlinear absorption effect can be ascribed to reverse saturable absorption (RSA) of HA, more specifically, the efficient absorption of the excited states of HA.

In addition, with the experimental apparatus, shown in Figure 3, we can also conveniently determine the effective absorption coefficient at the focus, α_{eff}. Experimentally, by fixing the sample at the focal position ($Z = 0$), we measured the incident energy E_i and the transmitted energy E_t. Then α_{eff} is determined by the relation $E_t/E_i = \exp(-\alpha_{eff}L)$, with L being the sample length. The result is presented in Figure 6a. α_{eff} evidently

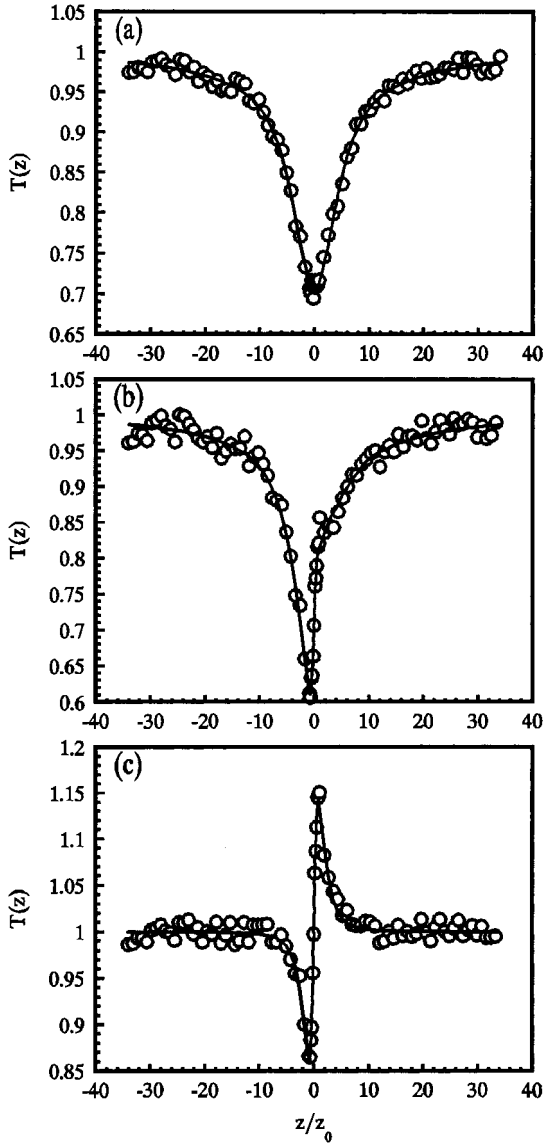

Figure 4. Typical (a) open aperture, (b) closed aperture, and (c) divided *Z*-scan data for HA at 0.53 μm. The solid lines are the theoretical fits. $I_0 = 25$ GW/cm^2.

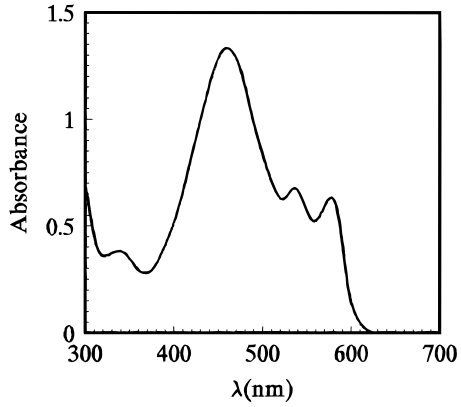

Figure 5. Linear absorption spectrum of a 2 mm thick HA solution in ethanol of 2.5×10^{-4} M concentration.

increases with I_0 at the lower irradiances (<5 GW/cm^2), whereas this increase becomes more moderate at the irradiances larger than 5 GW/cm^2.

The signal of the closed aperture *Z*-scan exhibits an asymmetrical valley configuration, which indicates serious perturbation of the nonlinear absorption effect on the closed aperture signal induced by purely nonlinear refraction (see Figure 4b). To simplify the analysis of experimental data, a divided *Z*-scan curve with the nearly symmetrical valley−peak configuration was obtained by the division of the closed aperture data by the open aperture ones correspondingly (see Figure 4c). Such a curve, which depends only on the nonlinear refraction under the certain approximation conditions,[16] indicates the presence of positive refraction nonlinearities in HA solution. By use of the equation[16,20]

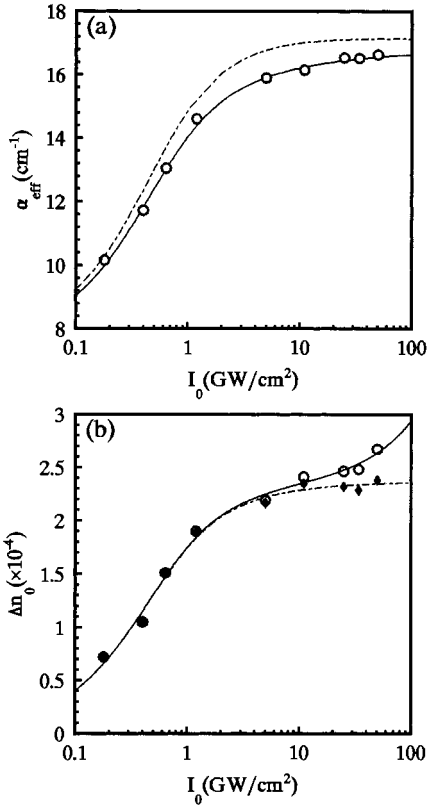

Figure 6. (a) Measured (○) and computed α_{eff} versus I_0 at 0.53 μm. The solid line and broken line represent the computed results using the five-level model and three-level model, respectively. (b) Measured (○) Δn_0 versus I_0 at 0.53 μm. The diamond symbols denote Δn_0 with the contribution of ethanol deducted as a function of I_0. The solid and broke lines represent the theoretical fits.

$$T(z) = 1 - \frac{4\langle\Delta\Phi_0\rangle(Z/Z_0)}{(Z^2/{Z_0}^2 + 9)(Z^2/{Z_0}^2 + 1)} \quad (1)$$

to fit the data of Figure 4c together with the relation

$$\Delta n_0 = \sqrt{2}\langle\Delta\Phi_0\rangle/(kL_{eff}) \quad (2)$$

we can determine the peak-on-axis index change at focus for each irradiance, shown in Figure 6b. In the preceding two equations, $\langle\Delta\Phi_0\rangle$ represents the time-averaged on-axis phase shift at focus, $k = 2\pi/\lambda$, is the magnitude of wave vector with λ being the laser wavelength, and $Z_0 = kw_0^2/2$ is the diffraction length of the beam with w_0 being the waist radius. As shown in Figure 6b, Δn_0 increases with increasing I_0. This increasing trend is maintained at high irradiance (>5 GW/cm^2) as well.

3.2. Time-Resolved Two-Color *Z*-Scan. *3.2.1. Z-Scans at Fixed Time Delays.* By fixing the time-delay stage at zero time delay and time delay of 100 ps, we measured the

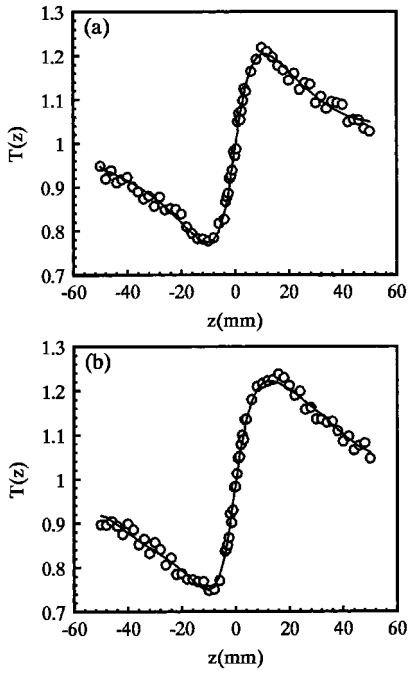

Figure 7. Signals of closed aperture two-color *Z*-scan at zero time delay (a) and a time delay of 100 ps (b) at $I_0 = 25$ GW/cm^2. The solid lines represent the theoretical results.

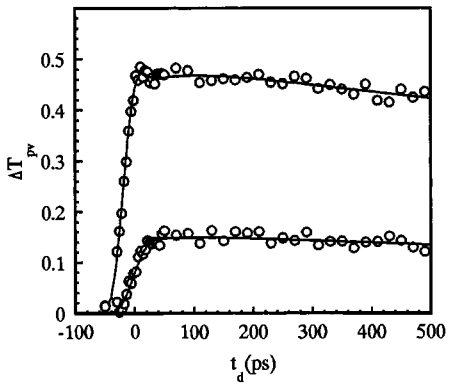

Figure 8. ΔT_{pv} versus t_d with the theoretical fit (solid line) for the HA sample at a peak-on-axis irradiance at focus of the excitation light of 25 GW/cm^2 (a) and 0.64 GW/cm^2 (b).

normalized transmittances as functions of the position of the sample, *Z*. The open aperture *Z*-scans showed the absence of any nonlinear absorption in HA. The signals of the closed aperture *Z*-scan, presented in Figure 7, are characterized by prefocal valleys followed by postfocal peaks, which imply the presence of positive nonlinear refraction for the two different time delays. These data are, thereby, similar to the single-beam *Z*-scan data. It is worth noting that the occurrence of the refractive nonlinearities at long time delay, when there is no temporal overlap between the probe and excitation pulses, indicates the evident contribution of a slow nonlinear mechanism to the decay of the nonlinearities in the HA sample.

3.2.2. Temporal Scans at Fixed Sample Positions. Fixing the sample at the positions of the peak transmittance, Z_p, and the most extreme valleys Z_V, determined in the preceding experiments (1), we scanned the time-delay stage and recorded the corresponding transmittances at each time delay t_d, referred to as $T(t_d,Z_p)$ and $T(t_d,Z_V)$, respectively. The difference between $T(t_d,Z_p)$ and $T(t_d,Z_V)$, $\Delta T_{pv}(t_d)$, is plotted versus t_d is shown in Figure 8. Because $\Delta T_{pv}(t_d)$ is directly proportional to the refractive index change,[13] it reflects the time evolution of the refractive nonlinearities of the sample. Figure 8 indicates that either at high excitation irradiance ($I_0 = 25$ GW/cm^2) or at low excitation irradiance ($I_0 = 0.63$ GW/cm^2), $\Delta T_{pv}(t_d)$ consists of a fast-growing and a very slow nonexponentially decaying tail, which lasts much longer than the laser pulse width.

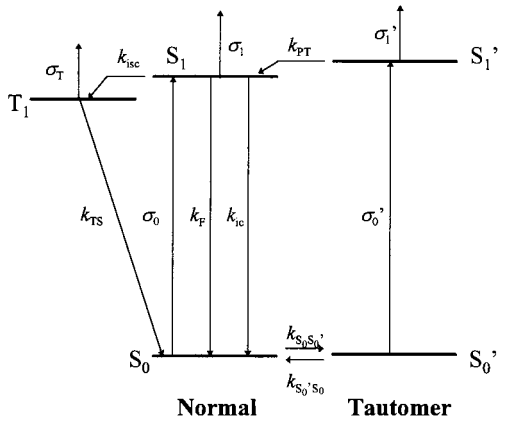

Figure 9. Five-level kinetic model of HA.

It should be pointed out that we did not observe the evident signal of the solvent, ethanol, in the experiment under identical experimental conditions. Therefore, the signals presented in Figure 7 and Figure 8 are due solely to the solute, HA.

4. Theory and Discussion

4.1. Five-Level Kinetic Model. For HA, there are two important photophysical processes that occur. First, HA undergoes an ESIPT with a rate comparable to the duration of the excitation pulse, resulting in a structural change from the tautomeric form to the normal form.[6] Second, both the normal and tautomerized species of HA exist in the ground state at equilibrium.[5] Because the structural changes between these two forms are so small, no significant differences in their electronic structures are evident.[5] Consequently, it is reasonable to assume that the ground states of the normal and tautomeric forms are nearly isoenergetic and equally populated. As a result of the above two points, we can develop the five-level model shown in Figure 9 to describe the photophysical behavior in HA.

When HA is excited by laser pulses in its resonant region, both the normal and tautomeric species in the ground states S_0 and S_0' are pumped to their first excited states S_1 and S_1', respectively. In the first excited state of tautomer S_1', the ESIPT, resulting in the relaxation process $S_1' \rightarrow S_1$ (k_{PT}),[5,7] occurs.[5] Because of the fast proton-transfer rate compared with those of the other decay pathways of S_1', it is the dominant relaxation pathway of S_1'. The excited state of the normal form, S_1, generally has three decay processes: intersystem crossing (k_{isc}) to the triplet state of the normal form T_1, and radiative (k_F) and nonradiative (k_{ic}) processes that return it to the ground state of the normal form, S_0. The population of T_1 is mainly depleted by nonradiative relaxation (k_{TS}) to S_0. In the ground state, it is assumed that a fast equilibrium between S_0 and S_0', with equal rate constants, $k_{S_0S_0'}$ and $k_{S_0'S_0}$ exists.

Higher excited manifolds, such as S_i, S_i', and T_i ($i > 1$), are not considered in our model, since the nonradiative relaxation from these higher excited states to S_1, S_1', and T_1 has been proven to be very fast relative to the time regime in which we are interested.[22] According to the model described above, we

write the rate equations for the five states as

$$\frac{\partial N_0}{\partial t} = -\frac{\sigma_0 I}{\hbar\omega}N_0 + (k_{ic} + k_F)N_1 + k_{S_0'S_0}N_0' - k_{S_0S_0'}N_0 + k_{TS}N_T \quad (3)$$

$$\frac{\partial N_0'}{\partial t} = -\frac{\sigma_0' I}{\hbar\omega}N_0' + k_{S_0S_0'}N_0 - k_{S_0'S_0}N_0' \quad (4)$$

$$\frac{\partial N_1}{\partial t} = \frac{\sigma_0 I}{\hbar\omega}N_0 + k_{PT}N_1' - \frac{N_1}{\tau_1} \quad (5)$$

$$\frac{\partial N_1'}{\partial t} = \frac{\sigma_0' I}{\hbar\omega}N_0' - k_{PT}N_1' \quad (6)$$

$$\frac{\partial N_T}{\partial t} = k_{isc}N_1 - k_{TS}N_T \quad (7)$$

where N_0, N_1, N_T, N_0', and N_1' are the population densities (molecules cm^{-3}) of S_0, S_1,T_1, S_0', and S_1', respectively, σ_0 and σ_0' are the absorption cross sections of S_0 and S_0' at the excitation laser wavelength, respectively, $\hbar\omega$ is the input excitation photon energy, I is the excitation irradiance, which is a function of the time t, the space coordination r, the position of the sample Z, and the propagation depth in the sample Z'. Thus, it can be written as $I(r,t,Z,Z')$.

In the rate equations, the term "$k_{TS}N_T$" might be neglected because the lifetime of the T_1 state ($\sim\mu$s[3]) is much longer than the time scale we are interested in.

Now, the boundary conditions of eqs 3−7 can be determined. In the initial time, only the ground states of the normal form (S_0) and tautomer (S_0') are populated with equal population densities N_{00}, $N_{00'}$, i.e., $N_{00} \approx N_{00'} \approx 7.5 \times 10^{16}$ cm^{-3} corresponding to the concentration of HA, 2.5×10^{-4} M. The population densities of the other three states are regarded as zero. The values of several parameters related to the rate equations are: $k_{isc} = 6.4 \times 10^8$ s^{-1},[3,5] $k_r + k_{ic} = 1.3 \times 10^8$ s^{-1},[5] $k_{S_0S_0} \approx k_{S_0S_0} \approx 5.0 \times 10^{10}$ s^{-1},[23] and $k_{PT} = 1.25 \times 10^{10}$ s^{-1}.[5] σ_0 and σ_0' are related by the relation $\sigma_0 + \sigma_0' = 2\sigma_{eff}$, where σ_{eff} is the effective absorption cross section of HA, determined by the linear spectrum. In the experiment, σ_{eff} is found to be 5.1×10^{-17} cm^2 at 0.53 μm.

With σ_0 or σ_0' known, the numerical solutions to the rate equations can be obtained by use of the fourth-order Runge−Kutta method.

Averaging the population density over t, r, and Z, gives the average population density for each state as

$$\langle N_i \rangle = \frac{\int_0^L dZ' \int_{-\infty}^{\infty} dt \int_0^{\infty} rN_i I\, dr}{\int_0^L dZ' \int_{-\infty}^{\infty} dt \int_0^{\infty} rI\, dr} \quad (8)$$

where N_i represents N_0, N_1, N_T, N_0', or N_1' which are functions of t, r, Z, and Z'.

4.2. Single-Beam *Z*-Scan. *4.2.1. The Absorption Cross Sections of S_0, S_0',* and S_1'. Because the rate of intersystem crossing ($S_1 \rightarrow T_1$), k_{isc}, is much smaller than the reciprocal of the laser pulse width, the triplet state T_1 is less populated within the excitation pulse duration relative to S_1 and S_1'. Therefore, its averaged population density is also much smaller than those of S_1 and S_1'. Hence, the principle mechanism causing RSA is the efficient absorption of S_1 and S_1'; the contribution of the T_1 state can be ignored. Verification for this argument is found in the computation results, shown in Figure 10 and will be discussed below. The depletion of the excitation irradiance is given by

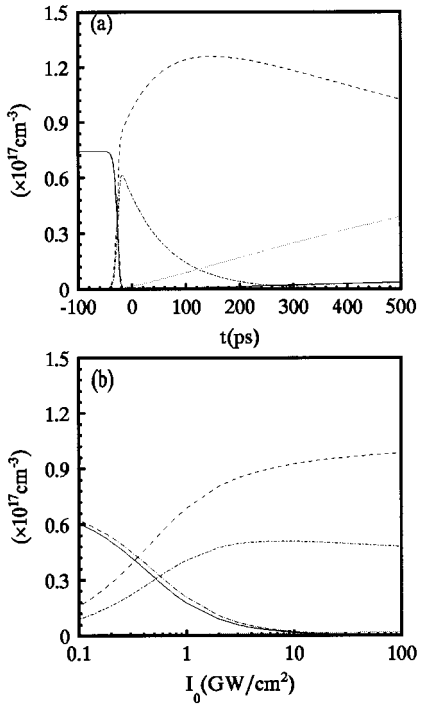

Figure 10. (a) Time evolution of the population densities of S_0 (—), S_1 (- - -), T_1 (• • •), S_0' (- • -), and S_1' (— - —). (b) Averaged population densities at focus of S_0 (—), S_1 (- - -), T_1 (• • •), S_0' (- • -), and S_1' (— - —) versus I_0.

TABLE 1: Absorption Cross Sections of S_0, S_0', and S_1'

I_0 (GW/cm^2)	0.18	0.40	0.64	1.2	5.0	11	25	34	50
σ_0 ($\times 10^{-17}$ cm^2)	5.7	5.8	6.1	5.7	6.0				
σ_0' ($\times 10^{-17}$ cm^2)	4.5	4.4	4.1	4.5	4.2				
σ_1' ($\times 10^{-17}$ cm^2)	8.6	7.1	7.7	8.0	7.6	7.5	7.9	7.7	7.9

$$\frac{\partial I}{\partial Z'} = -\alpha I \quad (9)$$

where $\alpha = \sigma_0 N_0 + \sigma_1 N_1 + \sigma_0' N_0 + \sigma_1 N_1$ is the transient absorption coefficient. σ_1 and σ_1' are the absorption cross sections of S_1 and S_1', respectively. σ_1 has been determined in our previous nanosecond studies to be 1.13×10^{-16} cm^2.[9]

The irradiance at the exit surface of the sample ($Z' = L$) is obtained by solving eq 9 numerically with σ_0 (or σ_0') and σ_1' known. Moreover, it will lead to the normalized transmittance of open aperture Z-scan after integration over the spatially and temporally Gaussian pulse

$$T(Z) = \frac{2\pi \int_{-\infty}^{\infty} dt \int_0^{\infty} rI(l, r, t, Z)\, dr}{E_0 \exp(-\alpha_0 L)} \quad (10)$$

where $E_0 = \pi^{3/2} w_0^2 I_0 t_0/2$ is the incident pulse energy with t_0 being the half width at 1/e pulse width.

σ_0, σ_0', and σ_1 are determined by the fits to the data of open aperture Z-scans at nine peak-on-axis irradiances at focus. Table 1 presents such a fit result, from which three conclusions can be drawn. First, the absorption cross section of S_0, σ_0, is larger than that of S_0', σ_0'. As a result, it can be expected that S_1 is more populated than S_1'. Such a deduction is also confirmed by the numerical simulation result obtained with eqs 3−7, shown in Figure 10a. Second, the absorption cross section of S_1, σ_1', is also slightly larger than that of S_1', σ_1'. Therefore, as a result

of the above two points, the efficient absorption of S_1 is the more important mechanism resulting in RSA than is that of S_1', although S_1' has the specific contribution to RSA. Third, both σ_1 and σ_1' are larger than σ_0 and σ_0'. This is the major reason for the occurrence of RSA in HA.

The effective absorption coefficient at focus, α_{eff}, should be paid special attention to. It can be reasonably considered to be the average value of the transient absorption coefficient α

$$\alpha_{eff} = \sigma_0\langle N_0(Z=0)\rangle + \sigma_1\langle N_1(Z=0)\rangle + \sigma_0'\langle N_0'(Z=0)\rangle + \sigma_1'\langle N_1'(Z=0)\rangle \quad (11)$$

where $\langle N_0(Z=0)\rangle$, $\langle N_1(Z=0)\rangle$, $\langle N_0'(Z=0)\rangle$, and $\langle N_1'(Z=0)\rangle$ represent the average population densities of S_0, S_1, S_0', and S_1' at focus, respectively. Equation 11 shows that α_{eff} is directly related to the average population densities of the four states. At the low irradiances, besides S_1 and S_1', S_0 and S_0' have contributions to α_{eff} because there is still significant population of these two ground states. With increasing I_0, $\langle N_1\rangle$ and $\langle N_1'\rangle$ increase, while $\langle N_0\rangle$ and $\langle N_0'\rangle$ decrease. Because the absorption cross sections of S_1 and S_1' are larger than those of S_0 and S_0', the increase will surpass the decrease in eq 11. Therefore, α_{eff} will increase with I_0. At higher intensities, both the S_0 and S_0' states are pumped to be nearly empty. In other words, only the contributions from S_1 and S_1' are the dominant factors governing the value of α_{eff}. In this case, as is shown in Figure 10b, $\langle N_1\rangle$ still increases slightly with increasing I_0, whereas $\langle N_1'\rangle$ shows a slight drop. As a result of the large cross section of S_1 compared with that of S_1', the increase of the term $\sigma_1\langle N_1\rangle$ still overcomes the decrease of the term $\sigma_1'\langle N_1'\rangle$. The overall effect is a slight increase of α_{eff} with I_0. Consequently, the experimental phenomenon, shown in Figure 6a, can be explained satisfactorily. Furthermore, with the mean values of σ_0, σ_0', and σ_1', presented in Table 1, we calculated α_{eff} as a function of I_0, drawn in Figure 6a as a solid line. The theoretical curve is in close agreement with the experimental one.

To further verify the completeness of the kinetic model, a series of contrast calculations were done based on a three-level model, in which the ESIPT process is ignored. That is, the excited state of the tautomer S_1' is not considered, and the ground states of both the normal form and tautomeric form are treated as one electronic state. Therefore, the three electronic states in this supposed model are the ground state, the first excited state, and the triplet state of the normal form of HA. Performing the computations analogous to those done for the five-level model, we obtained the theoretical curve of α_{eff} versus I_0, shown in Figure 6a at the broken line. The calculated values of α_{eff} are obviously larger than the experimental ones at high irradiances. Since under the three-level approximation, only the first excited state of the normal form, S_1, predominantly governs the absorption of HA, such a model overestimates the contribution of S_1 to α_{eff}. This implies that there might exist another excited state, which has an absorption coefficient less than that for S_1. In fact, by invoking the five-level model that involves the electronic states related to the tautomer, we can give the experiment a good explanation. Thus, such a contrasting computation definitely demonstrates that the five-level model is reliable enough to describe the photophysical processes of HA under the excitation of picosecond pulses. What is more, we verified the occurrence of ESIPT in HA.

4.2.2. The Refractive Nonlinearities of S_1 and S_1'. In general, the four states S_0, S_0', S_1, and S_1' make contributions to the nonlinear refraction in HA. At higher irradiances (>5 GW/cm^2), it is reasonable to neglect the contribution from the ground states, S_0 and S_0', because these two states are excited to be nearly empty under such irradiances. In addition, besides the contribution of the solute, HA, the contribution of the solvent, ethanol, should be included. By assuming that there is no interaction between the solute and solvent, we can write the total change in the refractive index as

$$\Delta n_0 = \frac{\chi_R^{(3)\prime}}{2n_0^2\epsilon_0 c} I_0 + \sigma_{r,S_1}\langle N_1\rangle + \sigma_{r,S_1'}\langle N_1'\rangle \quad (12)$$

The first term on the right-hand side of eq 12 represents the contribution of the solvent, where $\chi_R^{(3)\prime}$ is the real part of the third-order susceptibility of ethanol with a value of 5.8×10^{-22} m^2/V^2 determined by the single-beam *Z*-scan experiment. It hardly changes with I_0. The last two terms represent the contributions of the excited states of the normal and tautomeric forms, S_1 and S_1', respectively. The refractive nonlinearities of these two states are denoted by σ_{r,S_1} and $\sigma_{r,S_1'}$ (in cubic centimeters), respectively.

The fit to the experimental data, shown in Figure 6b, using eq 12 gives σ_{r,S_1} and $\sigma_{r,S_1'}$ values of 1.8×10^{-21} and 1.2×10^{-21} cm^3, respectively. The fitted curve is presented in Figure 6b as a solid curve. It shows close agreement with the experiment even at lower irradiance, which implies that the contributions of the two ground states, S_0 and S_0', can be ignored for all irradiances used in this experiment. In other words, the refractive nonlinearities of HA mainly originate from the contributions of the two excited states S_1 and S_1'.

To explicitly explain the experimental result shown in Figure 6b, we subtract the contribution of ethanol from the total index change and obtain a curve only representing the refractive nonlinearities of HA, also shown in Figure 6b with a diamond symbol. Such a curve indicates that evidently Δn_0 increases with I_0 at low irradiance, whereas it is almost independent of I_0 at irradiances larger than 5 GW/cm^2. The result can be explained upon inspection of eq 12. As is shown in Figure 10b, the time-averaged population densities of both S_1 and S_1' distinctly increase with increasing I_0 at low irradiances, while these two states become saturated at high irradiances.

4.3. Time-Resolved Two-Color *Z*-Scan. In the case of the time-resolved two-color *Z*-scan measurement, there exist two laser beams, the excitation beam and probe beam. For the probe beam, with the approximation of a thin sample and a slowly varying envelope, the Maxwell equations can be separated into an equation for the amplitude $|E_p|$ and an equation for the phase Φ_p.[13] The HA molecule exhibits neither linear absorption at the wavelength of the probe beam (1.06 μm) nor degenerate ($h\omega_p + h\omega_p$) or nondegenerate ($h\omega_p + h\omega_e$) two-photon absorption. This absence of the probe effect on nonlinear absorption is due to very weak irradiance by the probe beam. Hence, we can further express these two equations as

$$\frac{\partial|E_p|}{\partial Z'} = 0 \quad (13)$$

$$\frac{\partial\Phi_p}{\partial Z'} = k_p\Delta n(\omega_p,\omega_e) \quad (14)$$

where ω_p and ω_e, are the frequencies of the probe and excitation beams, respectively, k_p is the magnitude of the wave vector of the probe beam, $\Delta n(\omega_p, \omega_e)$ represents the total change in the refractive index at ω_p upon excitation. It should consist of contributions from both the ethanol solvent and the HA solute, including the ground states (S_0, S_0'), singlet excited states (S_1,

S_1'), and triplet state (T_1). As with single-beam *Z*-scan, it is credible to neglect the contributions of the ground states S_0 and S_0'. In addition, no two-color *Z*-scan signal for neat ethanol was observed. Therefore, the contribution of ethanol to the total index change can be ignored. Under these approximations, the total change of refractive index is expressed by

$$\Delta n(\omega_p, \omega_e) = \Delta n_{S_1} + \Delta n_{S_1'} + \Delta n_{T_1} = \sigma_{r,S_1}(\omega_p)N_1 + \sigma_{r,S_1'}(\omega_p)N_1' + \sigma_{r,T}(\omega_p)N_T \quad (15)$$

where the terms on the right-hand side of the equation represent the contributions of S_1, S_1', and T_1, denoted by $\sigma_{r,S_1'}$, $\sigma_{r,S_1'}$, and $\sigma_{r,T}$, respectively. N_1, N_1', and N_T and are determined by the rate equations (eqs 3−7). The irradiance of the excitation beam is also governed by eq 9 with the boundary condition

$$I(Z' = 0) = \frac{I_0}{1 + (Z + Z_c)^2/{Z_0}^2} \times \exp\left\{ - \frac{2r^2}{{w_0}^2[1 + (Z + Z_c)^2/{Z_0}^2]} - \frac{(t + t_d)^2}{{t_0}^2} \right\} \quad (16)$$

where Z_c is the distance between the waist positions of the two beams due to the chromatic aberration of lens L1 and t_d is the time delay of the probe pulse relative to the excitation pulse.

Following similar derivation procedures as described in ref 13, we can write the normalized transmittance of time-resolved closed aperture *Z*-scan as

$$T(t_d, Z) = \frac{\int_{-\infty}^{\infty} dt \int_0^{r_a} r\, dr |E_a|}{\int_{-\infty}^{\infty} dt \int_0^{r_a} r\, dr |E_a\,(I_0 = 0)|} \quad (17)$$

where r_a is the aperture radius and E_a is the electric field profile of the probe beam at the aperture plane, determined by the Hugens−Fresnel propagation integral[13,24]

$$E_a(r, t, Z) = \frac{2\pi}{i\lambda_p(d - Z)} \exp\left[\frac{i\pi r^2}{\lambda_p(d - Z)}\right] \int_0^{\infty} r'\, dr' \times E_p(r', t, Z, Z' = L) \exp\left[\frac{i\pi r'^2}{\lambda_p(d - Z)}\right] J_0\left[\frac{i\pi r r'}{\lambda_p(d - Z)}\right] \quad (18)$$

where *d* is the distance between the aperture and the focal plane of the excitation beam, λ_p is the wavelength of the probe beam, J_0 is the Bessel function of zeroth order, and $E_p(r,t,Z,Z' = L)$ is the field at the exit surface of the sample, which can be completely determined by eqs 13 and 14. Taken as a Gaussian in space and time, it is given by

$$E_p(r', t, Z, Z' = L) = \frac{E_{0p}}{\sqrt{1 + Z^2/{Z_{0p}}^2}} \exp\left[- \frac{r^2}{{w_{0p}}^2(1 + Z^2/{Z_{0p}}^2)} \times \left(1 + \frac{iZ}{Z_{0p}}\right) - \frac{t^2}{2{t_0}^2} \right] \exp\left[-i \tan^{-1}\left(\frac{Z}{Z_{0p}}\right) \right] \exp(i\Delta\Phi(Z'=L)) \quad (19)$$

where $Z_{0p} = \pi {w_{0p}}^2/\lambda_p$ is the diffraction length of the probe beam with w_{0p} being the waist radius.

Then the difference in the peak-to-valley normalized transmittance can be further calculated with eq 17

$$\Delta T_{pv}(t_d) = \pm[T(t_d, Z_p) - T(t_d, Z_v)] \quad (20)$$

The sign of ΔT_{pv} is determined by the sign of $Z_p - Z_v$.

At the zero time delay, we can ignore the contribution of the triplet state T_1. In this case, the best fit to the experimental data shown in Figure 7a using eq 17 gives: $\sigma_{r,S_1} = 9.8 \times 10^{-22}$ cm^3 and $\sigma_{r,S_1'} = 7.4 \times 10^{-22}$ cm^3.

It is clear that the contribution of T_1 becomes evident at much longer time delay because of its significant population. Therefore, the evolution of ΔT_{pv} can provide useful information about the refractive nonlinearity of this state. In fact, with σ_{r,S_1} and $\sigma_{r,S_1'}$ known, $\sigma_{r,T}$ can be determined by the fit to the experimental curve $\Delta T_{pv}(t_d)$ at $I_0 = 25$ GW/cm^2 using eq 20. Such a fit gives the result $\sigma_{r,T} = 6.1 \times 10^{-22}$ cm^3.

Using these fit results, σ_{r,S_1}, $\sigma_{r,S_1'}$, and $\sigma_{r,T}$ we calculated the theoretical curve of the closed aperture two-color *Z*-scan at the time delay of 100 ps ($I_0 = 25$ GW/cm^2 $\Delta T_{pv}(t_d)$ and at $I_0 = 0.64$ GW/cm^2. They are in good agreement with the experimental data (see Figures 7b and 8).

Consequently, on the basis of the experimental results of time-resolved two-color *Z*-scans, we determined the refractive nonlinearity of the triplet state T_1 as well as those of the singlet excited states S_1 and S_1'. Moreover, it can be expected that the separated study of nonlinear refraction and dynamics of T_1 will become possible with long enough time delay (i.e., $t_d \gg 1/k_{ST}$), when T_1 is efficiently populated at such long time delays whereas S_1 and S_1' are depleted to be almost empty.

The explanation for the very slow decay of ΔT_{pv}, representing the refractive nonlinearities, involves the kinetics of HA. It is clear from eq 15 that the nonlinear refraction is governed by the population densities of S_1, S_1', and T_1. That is, its decay is directly dependent on the population and relaxation of these electronic states. Therefore, we conclude that at the time delays smaller than the lifetime of S_1' (80 ps), the contributions of S_1 and S_1' are the dominant mechanisms, other than that of T_1, causing the nonlinear refraction because T_1 has a rise time of ∼1 ns and is much less populated in contrast to the other two states within this time region. When the time delay is larger than 80 ps, the nonlinear refraction largely comes from the contribution of S_1 within the upper limit of time delay in our experiment (500 ps), although the contribution of T_1 becomes more and more evident with the increase of t_d.

4.4. Can Other Models Describe the Kinetics of HA Well? It is evident that there are several possible schemes to describe the kinetics of HA other than the one developed in this paper. Can the experimental data be explained well by these models? To answer this question, we have tried two possible models and done the similar calculations and analysis.

The first model we tried is shown in Figure 11. Assume that the proton transfer occurs in an S_1 state, and this proton transfer is coupled to intersystem crossing to produce the triplet state of tautomer, T_1', and S_1' just forms T_1'. In such a model, S_1' is a strong fluorescent state with a long lifetime (∼nanoseconds) instead of S_1, and T_1' is populated rather than T_1. The rate equations can be obtained by rewriting eqs 3−7 based on such a scheme. The several parameters relevant to these rate equations are such determined. The values of k_{isc}, $k_r + k_{ic}$, $k_{S_0'S_0}$, $k_{S_0S_0'}$, and k_{PT}, and are the same as those for the original model. The absorption cross sections of S_1' (σ_1') and T_1' (σ_T') (equivalent to σ_1 and σ_T in the original model, respectively) are given values of 1.13×10^{-16} cm^2 and 8.15×10^{-17} cm^2, respectively.[9] Following similar procedures as those described

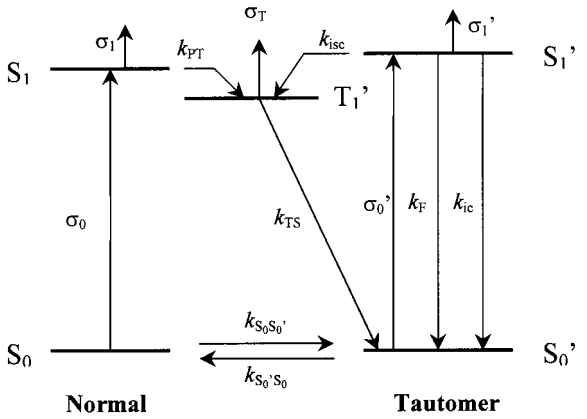

Figure 11. Possible kinetics scheme for HA used in the contrast computation.

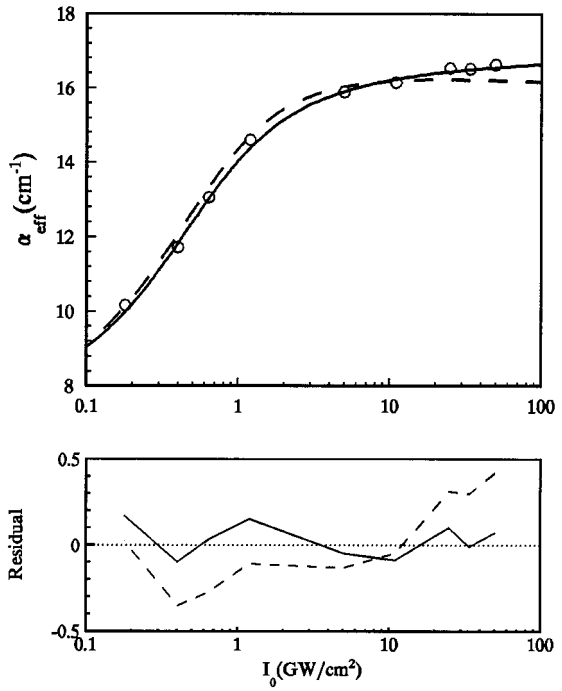

Figure 12. Computed α_{eff} versus I_0 at 0.53 μm, together with the experimental data (○). The solid line and broken line represent the computed results using the model shown in Figure 9 and the model shown in Figure 11, respectively. Residuals for the theoretical curves are shown at the bottom.

for the original model shown in Figure 9, we obtained the theoretical curve of α_{eff} versus I_0, shown in Figure 12 together with that based on the original model for comparison. It is clear that the theoretical curve does not match the experiment well. The reason for this is that the evolution of the population densities (see Figure 13) is quite different from those based on the original model. By comparing Figure 13 with Figure 10, one can easily find that there are two distinct differences between the two cases. First, the triplet state is populated more evidently for this model than that for the model shown in Figure 9 within the time scale of interest. Another difference comes from the distribution of the population densities of S_1 and S_1'.

In addition, as shown in Figure 14, the fit of the experimental curve, ΔT_{pv} versus t_d, is also not satisfactory. Much deviation occurs in the long time delay regime partly because of overestimating the contribution of the triplet state relative to the theoretical curve based on the original model. Therefore, the model shown in Figure 11 is not pertinent to describe the kinetics of HA.

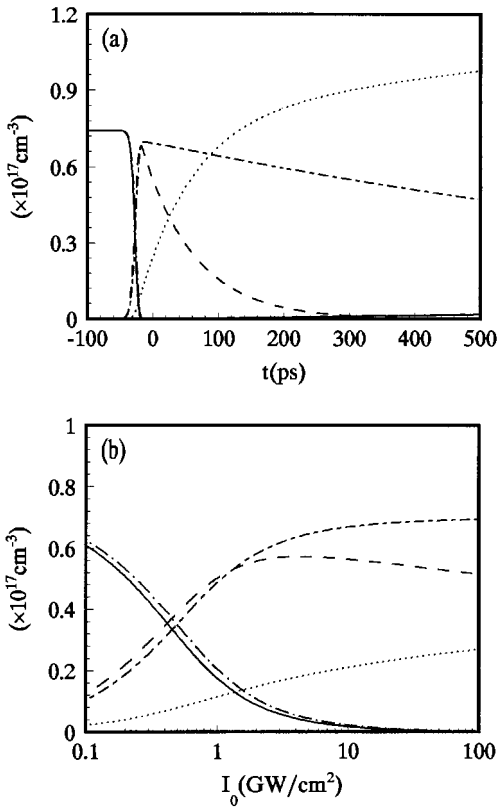

Figure 13. (a) Calculated time evolution of the population densities of S_0 (—), S_1 (- — -), S_0' (- · -), S_1' (— - —), and T_1 (· · ·) using the model shown in Figure 11. (b) Calculated average population densities at focus of S_0 (—), S_1 (- — -), S_0' (- · -), S_1' (— - —), and T_1 (···) versus I_0 using the model shown in Figure 11.

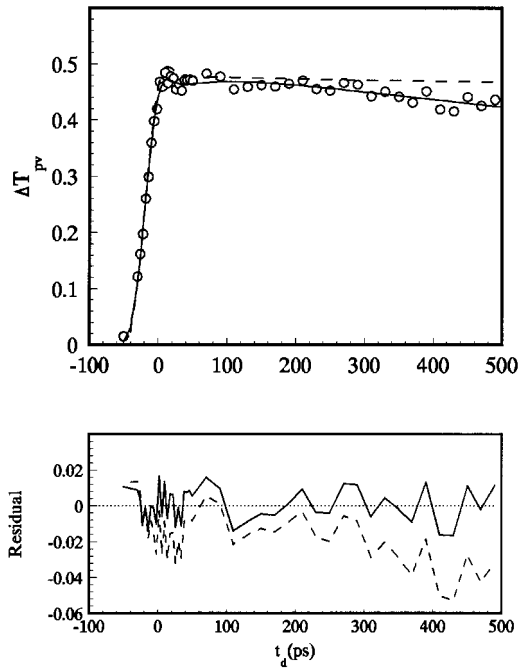

Figure 14. Theoretical fit (- — -) of the experimental curve of ΔT_{pv}-(t_d) (I_0 = 25 GW/cm^2) using the model shown in Figure 11, together with the fit using the model shown in Figure 9 (—). Residuals for the fitted curves are shown at the bottom.

We also tried another possible model; i.e., S_1' undergoes back proton transfer to the triplet state of the normal form of HA, T_1. On the basis of such a model, the fits to the experimental

data shown in Figures 6 and 8 are still not satisfactory. This suggested that this scheme is not a good model for HA.

After performing the above computations, we think that the original model shown in Figure 9 is complete enough to describe the kinetics of HA.

In the end, it is still necessary for us to point out that the observed results are insensitive to the presence of molecular oxygen, although HA has an enormous yield of singlet oxygen ($^1O_2$) (~76%). It has been demonstrated that $^1O_2$ is formed by energy transfer between the excited triplet state of HA (T_1) and the ground state of oxygen:[3]

$$T_1 + {}^3O_2 = {}^1O_2 + S_0$$

This process is controlled by molecular diffusion rates and is closely related to the molecular oxygen concentration. At 1 atm, the rate of energy transfer between the ground-state oxygen and T_1, k_{ET}, is estimated to be 10^6-10^8 s^{-1} with the presence of saturated oxygen.[3] Because HA is nonphosphorescent, such an energy transfer process can be regarded as the dominant pathway for deactivation of T_1 relative to the intersystem crossing. In addition, because this process is much slower than the time scale of interest (less than subnanosecond), the molecules in the T_1 state cannot return to the S_0 state within the subnanosecond time regime. So, we neglect the term "$k_{TS}N_T$" in eq 7. When the molecular oxygen concentration decreases due to a deoxygenating process, the energy transfer (k_{ET}) will become slower compared with that without deoxygenating. That is to say, the lifetime of T_1 will be at least longer than tens of nanoseconds. So, in this case, the decay pathway of T_1, k_{ST}, can also be ignored within the subnanosecond time regime. On the other hand, because the process involved in production of the singlet oxygen has less influence on the population and decay of the singlet states including exited states and ground states, the kinetics of HA hardly changes with the decrease of concentration of the molecular oxygen in the HA solution. Furthermore, because the optical nonlinearity of HA is closely related to the population densities of the electronical states (see eqs 11, 12, and 15) and thus the kinetics of HA, the amount of molecular oxygen dissolved in the HA solution has less effect on optical nonlinearities of HA.

Experimentally, we deoxygenated the sample by bubbling argon for 1 h and performed the same experiments to measure the optical nonlinearities of HA as described in this paper. The nearly same results were obtained as those for the nondeoxygenated sample. So, both the theoretical and experimental results demonstrate that the observed nonlinear optical properties of HA are insensitive to the presence of molecular oxygen.

5. Conclusion

In conclusion, we have been the first, to our knowledge, to study the optical nonlinearities (including nonlinear absorption and nonlinear refraction) of HA and the temporal properties of HA in its resonant region using single-beam *Z*-scan and time-resolved two-color *Z*-scan techniques. The main results are summarized as follows.

(A) HA exhibits a reverse saturable absorption effect, which can be ascribed to the efficient absorption of the excited states of both the normal and tautomeric forms, S_1 and S_1'. But the contribution of S_1 is the dominant mechanism.

(B) At lower irradiance, the change in the refractive index of HA, Δn_{HA}, increases with increasing I_0, while it is independent of I_0 at higher irradiance. The explanation for this experimental phenomenon is understood through consideration of the kinetics of HA. The time-averaged population densities of both S_1 and S_1' increase with I_0 at low irradiance until the population of these two states becomes saturated.

(C) Time-resolved two-color *Z*-scan allows for the study of the nonlinear refraction of the triplet state of the normal form of HA and of the singlet excited states of both the normal and tautomeric forms. Furthermore, this time-resolved technique gives important information about the temporal response of refractive nonlinearities of the sample. The very slow decay of refractive nonlinearities is attributed to the contributions of S_1, S_1', and T_1, dependent on their own rise times and lifetimes.

(D) An original five-level kinetic model has been developed to describe the photophysics of HA. This model explains the experiment satisfactorily. The theoretical results show remarkable agreement with experiment. Moreover, comparison of the computations using the five-level model and other models, including a three-level model, clearly demonstrate the completeness of the five-level model. In other words, we verified that HA undergoes ESIPT upon excitation, and such an ESIPT should be coupled between the first excited states of normal and tautomeric forms of HA. Furthermore, we obtained the cross sections of S_0, S_0', and S_1' and the refractive nonlinearities of S_1, S_1, and T_1. In summary, both the theoretical and experimental results suggest that the optical nonlinearities of HA are closely related to its photophysical processes involved in ESIPT.

Acknowledgment. This research was supported by the National Science Foundation of China. The authors are most grateful to Professor Norbert F. Scherer (Department of Chemistry, University of Chicago) for several valuable discussions. We sincerely thank Bret Flanders for his helpful suggestion and careful proofing of this paper. We also thank the Institute of Photographic Chemistry, Academia Sinica, China for supplying HA sample for our experiments.

References and Notes

(1) Hu, Y. Z.; An, J. Y.; Qin, L.; Jiang, L. J. *J. Photochem. Photobiol., A* **1994**, *78*, 247.

(2) English, D. S.; Das, K.; Zenner, J. M.; Zhang, W.; Kraus, G. A.; Larock, R. C.; Petrich, J. W. *J. Phys. Chem. A* **1997**, *101*, 3235.

(3) Diwu, Z.; Lown, J. W. *J. Photochem. Photobiol. A* **1992**, *64*, 273.

(4) Fehr, M. J.; Carpenter, S. L.; Wannemuehler, Y.; Petrich, J. W. *Biochemistry* **1995**, *34*, 15845.

(5) Das, K.; English, D. S.; Fehr, M. J.; Smirnov, A. V.; Petrich, J. W. *J. Phys. Chem.* **1996**, *100*, 18275.

(6) Das, K.; English, D. S.; Petrich, J. W. *J. Am. Chem. Soc.* **1997**, *119*, 2763.

(7) Das, K.; English, D. S.; Petrich, J. W. *J. Phys. Chem. A* **1997**, *101*, 3241.

(8) Das, K.; Dertz, E.; Paterson, J.; Zhang, W.; Kraus, G. A.; Petrich, J. W. *J. Phys. Chem. B* **1998**, *102*, 1479.

(9) Shang, X. M.; Liu, Y. Q.; Tang, G. Q.; Zhang, G. L.; Chen, W. J. *J. Opt. Soc. Am. B* **1998**, *15*, 1502.

(10) Hofer, T.; Kruck, P.; Kaiser, W. *Chem. Phys. Lett.* **1994**, *224*, 411.

(11) Hofer, T.; Kruck, P.; Elsaesser, T.; Kaiser, W. *J. Phys. Chem.* **1995**, *99*, 4380.

(12) Shang, X. M.; Tang, G. Q.; Zhang, G. L.; Liu, Y. Q.; Chen, W. J.; Yang, B. Z.; Zhang, X. Q. *J. Opt. Soc. Am. B* **1998**, *15*, 854.

(13) Wang, J.; Sheik-Bahae, M.; Said, A. A.; Hagan, D. J.; Van Stryland, E. W. *J. Opt. Soc. Am. B* **1994**, *11*, 1009.

(14) Tseug, K. Y.; Wong, K. S.; Wong, G. K. L. *Opt. Lett.* **1996**, *21*, 180.

(15) Brochard, P.; GrolierMazza, V.; Cabanel, R. *J. Opt. Soc. Am. B* **1997**, *14*, 405.

(16) Sheik-Bahae, M.; Said, A. A.; Wei, T. W.; Hagan, D. J.; Van Stryland, E. W. *IEEE J. Quantum Electron.* **1990**, *26*, 760.

(17) Said, A. A.; Sheik-Bahae, M.; Hagan, D. J.; Wei, T. H.; Wang, J.; Young, J.; Van Stryland, E. W. *J. Opt. Soc. Am. B* **1992**, *9*, 405.
(18) Said, A. A.; Wamsley, C.; Hagan, D. J.; Van Stryland, E. W.; Reinhardt, B. A.; Roderer, P.; Dillard, A. G. *Chem. Phys. Lett.* **1994**, *228*, 646.
(19) Cheung, Y. M.; Gayen, S. K. *J. Opt. Soc. Am. B* **1994**, *11*, 636.
(20) Hein, J.; Bergner, H.; Lenzner, M.; Rentsch, S. *Chem. Phys.* **1994**, *179*, 543.
(21) Wood, G. L.; Miller, M. J.; Mott, A. G. *Opt. Lett.* **1995**, *20*, 973.
(22) Schafer, F. P., Ed. Principle of dye laser operation. In *Dye Laser*; Topic in Applied Physics 1; Springer: Berlin, 1973; Sections 1 and 3, p 28.
(23) Borgis, D.; Tarjus, G.; Azzouz, H. *J. Phys. Chem.* **1992**, *96*, 3188.
(24) Gaskill, J. D. *Linear Systems, Fourier Transform, and Optics*; Wiley: New York, 1978.